The Low-Latitude Ionosphere Sensor Network: Initial results

C. E. Valladares[1] and J. L. Chau[2]

Received 31 December 2011; revised 27 March 2012; accepted 28 March 2012; published 18 May 2012.

[1] The Low-Latitude Ionospheric Sensor Network (LISN) is a distributed observatory designed to nowcast the state and dynamics of the low-latitude ionosphere and to develop forecasts of the electric fields, densities, and equatorial spread F over the South American continent. The LISN observatory consists of three different types of instruments: GPS receivers, fluxgate magnetometers, and vertical incidence pulsed ionospheric radar (VIPIR) ionosondes. This report provides a succinct summary of recent observations obtained using the LISN GPS receivers and complemented with measurements from other instruments and GPS receivers that operate in South America. More specifically, the following are shown here: (1) observations of total electron content (TEC) enhancements that occur near local midnight, (2) maps of TEC perturbations associated with the passage of traveling ionospheric disturbances over South America, and (3) statistics of TEC depletions for 2 years of low solar activity. Near-midnight TEC enhancements consist of sudden increases in TEC that occur after sunset at low latitudes on 30% of the days. These TEC enhancements last for several hours and can have amplitudes between 1 and 50 TEC units. On 11–12 March 2011 the largest TEC enhancement was observed in South America at times when the Jicamarca incoherent scatter radar operated and observed peak densities above 10^6 el/cc at 300 km altitude. It is suggested that a combination of zonal electric fields and meridional neutral winds are able to redistribute the plasma along the field lines and create regions of enhanced TEC. Maps of TEC perturbations associated with the passage of gravity waves (GWs) over South America have been used to measure the phase velocity and direction of propagation of GWs. The large number of GPS receivers over South America has allowed us to record bubble events for every day during 2008 and 2009. It was found that the number of TEC depletion detections varies with a periodicity of 28 days. It is mentioned how these new observations and the installation of the last four VIPIR ionosondes will lead to new discoveries in the near future.

Citation: Valladares, C. E., and J. L. Chau (2012), The Low-Latitude Ionosphere Sensor Network: Initial results, *Radio Sci.*, *47*, RS0L17, doi:10.1029/2011RS004978.

1. Introduction

[2] The main goal of the Low-Latitude Ionospheric Sensor Network (LISN) project is to establish a permanent array of instruments across the South American continent to investigate the complex day-to-day variability and the extreme state of disturbance that occurs in the equatorial ionosphere nearly every day after sunset. The LISN observatory is composed of three different types of instruments: GPS receivers, fluxgate magnetometers and vertical incidence pulsed ionospheric radar (VIPIR) ionosondes. All the instruments of the LISN distributed observatory provide nearly real-time observables (nowcast) to the Aeronomy community using a server located at Lima, Peru. The rationale behind the real-time measurements is to develop a short-term (60 min) predictive model of the ionosphere (forecast) based on real-time data ingestion, tomography density reconstruction, and assimilation techniques. At the time of writing this scientific report (30 November 2011) 45 dual-frequency GPS receivers, 5 magnetometers and 1 VIPIR ionosonde were part of the LISN network. Three magnetometers are installed and operating in the cities of Leticia, Colombia, Puerto Maldonado, Peru and at El Leoncito observatory in Argentina. Two other magnetometers are installed at the cities of Alta Floresta and Cuiaba, both in Brazil forming another baseline able to provide electric fields at the center of the continent. The first VIPIR ionosonde was placed near the magnetic equator in the city of Puerto Maldonado in Peru in October 2010. Four more ionosondes will be placed closely aligned with the magnetic field line that crosses the magnetic equator near 67° W longitude.

[1]Institute for Scientific Research, Boston College, Chestnut Hill, Massachusetts, USA.

[2]Radio Observatorio de Jicamarca, Instituto Geofísico del Perú, Lima, Peru.

Corresponding author: C. E. Valladares, Institute for Scientific Research, Boston College, St. Clements Hall #414, Chestnut Hill, MA 02467, USA. (cesar.valladares@bc.edu)

0048-6604/12/2011RS004978

[3] One of the objectives of the LISN observatory is to provide the necessary tools to study the ionospheric disposition and the seeding conditions for the initiation of equatorial spread F (ESF). ESF is one of the oldest unsolved problems in low-latitude aeronomy. Nevertheless, it is presently known that ESF consists of a gravitational overturn of the bottomside plasma that follows the physics of the Rayleigh-Taylor instability (RTI). The low-density plasma intrudes into the topside creating regions of plasma depletions that originate the appearance of plasma structures and irregularities during the nighttime [*Woodman and LaHoz*, 1976]. Plasma depletions, also named plasma bubbles or radar plumes, have been detected with radars, imagers, instruments on board satellites, and GPS receivers. The latter can provide complementary views of the integrated amount of plasma depleted within the bubbles. The low-latitude ionosphere also contains other types of irregularities such as bottomtype and bottomside layers [*Hysell and Burcham*, 1998] detected with coherent radars. Not well known, but still unexplained, are bottomside sinusoids (BSS) [*Valladares et al.*, 1983] that produce weak to strong UHF scintillations and are probably associated with a nonlocal development of the RTI.

[4] Due to the slow growth rate of the RTI (tens of minutes) *Röttger* [1973] suggested that GWs could act as a seed to initiate the onset of plasma bubbles. Lately, new evidence has emerged that favor the seeding effects of GWs to explain several features of the seasonal/longitudinal distribution of ESF occurrence [*Tsunoda*, 2010a, 2010b] and Digisonde observations from Brazil [*Abdu et al.*, 2009]. The current understanding holds that both favorable ionospheric conditions [*Farley et al.*, 1970; *Sultan*, 1996] and an initial seed perturbation on the bottomside are necessary to create channels of depleted plasma. In addition to GWs two new theories have been proposed to explain plasma bubbles: the wind-driven gradient drift instability [*Kudeki et al.*, 2007] and the altitude modulated E_s layer that creates a large-scale wave structure [*Tsunoda*, 2005, 2006]. These two mechanisms offer large growth rates that clearly rival the generalized RTI seeded by GWs. However, no definitive proof exists of any one being the dominant mechanism, or if all 3 can coexist or act at different local times, locations, or magnetic conditions.

[5] Another key point about the ESF phenomenon is the nonlocal nature of the plasma bubbles. It is the whole flux tube that becomes unstable (encompassing the E and F regions and the plasmasphere), consequently multipoint observations especially during the early phases of ESF development have been always desired but conducted only during a few dedicated campaigns [*Reinisch et al.*, 2005].

[6] This scientific report aims to point out how the LISN distributed observatory with its unique regional coverage and complementary instrumentation can probe the undisturbed low-latitude ionosphere prior to the initiation of ESF and detect the characteristics and morphology of GWs that can seed plasma bubbles. It is also indicated how the LISN observatory can detect the extension and duration of regions populated by total electron content (TEC) depletions. In addition, it shows how TEC values measured with the LISN GPS receivers and others that operate in South America can be used to diagnose the dynamics of the low-latitude ionosphere that drives the formation of large TEC enhancements that occur near midnight. Although this report is focused on the undisturbed low-latitude ionosphere prior to the initiation of ESF and the detection of TEC depletions, LISN instrumentation are being also important for other related topics. Two of these topics are (1) the low-latitude ionosphere behavior during sudden stratospheric warming (SSW) events and (2) the electron density structure of the valley region. In the former, *Goncharenko et al.* [2010] using GPS data from the LISN network have found a strong daytime ionospheric response to SSWs. This response is characterized by a semidiurnal character, large amplitude, and persistence of perturbations for up to 3 weeks after the peak in high-latitude stratospheric temperatures. These results are in good correspondence with the electric field perturbations observed over Jicamarca during SSW events [e.g., *Chau et al.*, 2009a, 2010]. The ionospheric perturbations at the lower latitudes usually begin a few days after the peak in stratospheric temperature and are observed as an enhancement of the equatorial ionization anomaly (EIA) in the morning sector and a suppression of the EIA in the afternoon sector. The latter studies have been performed using the VIPIR system while it was operating at Jicamarca. Combining Jicamarca VHF observations of 150 km echoes and VIPIR results, *Chau et al.* [2009b] were able to find a good indication that the 150 km echoes occur in a region with high variability in horizontal and vertical space as well as in time.

2. LISN GPS Receivers

[7] Figure 1 shows the geographic location of 45 dual-frequency GPS receivers that belong to the LISN observatory and are presently managed by the Institute of Scientific Research of Boston College. These receivers possess Internet connectivity to upload several real-time observables, such as code, phase, amplitude scintillations, and position to a central server that is located at the headquarters of the Instituto Geofisico del Perú, in Lima. Typical cadence time for data transfers is 15 min. The GPS information is stored, processed and displayed in the LISN web page and then retransmitted to another computer system at Boston College. This system is dedicated to produce regional plots of the TEC values, scintillations, TEC depletions associated with equatorial plasma depletions and TEC perturbations produced by the passage of traveling ionospheric disturbances (TID).

2.1. Observations of TEC Enhancements

[8] TEC values measured with 3 of the LISN GPS receivers on 3 different days are presented in Figure 2. This figure shows the TEC values measured at Puerto Maldonado on 13–14 October 2008 (Figure 2a), at Huancayo on 11–12 March 2011 (Figure 2b), and at Alta Floresta on 21–22 March 2011 (Figure 2c). These three stations are located close to the magnetic equator. The common feature in all three panels of Figure 2 is the sudden increase in the local TEC occurring 2–3 h after sunset and extending for a few hours before and after midnight. As shown below, TEC enhancements can also be observed at magnetic latitudes as high as 10°. The different traces seen in all three frames correspond to the TEC values observed using signals from different GPS satellites. At low latitudes, GPS receivers commonly track and lock to signals from 8 to 12 GPS

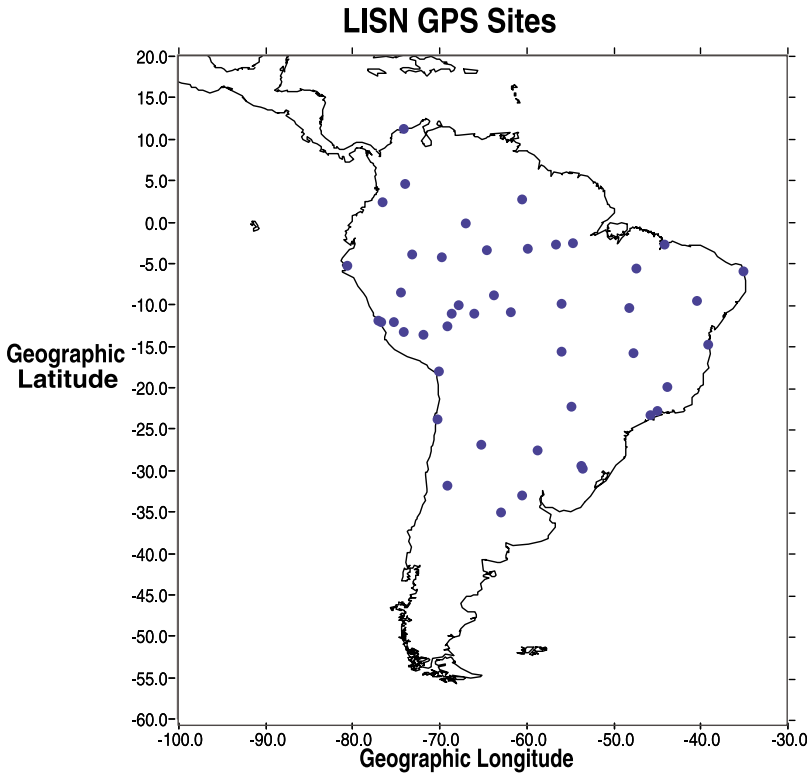

Figure 1. Locations of GPS receiver stations installed by the LISN project in the South American continent.

satellites simultaneously. In this publication, we suggest that near-midnight TEC enhancements are produced by the transport of plasma along field lines from latitudes between 15° and 25° to equatorial latitudes. It is also indicated that the presence of a meridional wind can modify the final location of the region of enhanced TEC values.

[9] The TEC values presented here were computed using the differential phase and pseudorange values of both L1 and L2 frequency signals [*Sardón and Zarraoa*, 1997] and leveling the differential phase to the average differential code values to eliminate the 2π phase ambiguity. The absolute values of TEC were then calculated by introducing the differential satellite biases published by the University of Bern and calculating the receiver bias by a minimization process of the TEC variability between 0200 and 0600 local time [*Doherty et al.*, 2004]. The absolute precision of the TEC measurements is affected by the errors in the calculation of the receiver bias, the uncertainties in the leveling process, and the errors of the satellite biases. All these absolute errors can add up to 1–2 TEC units. However, TEC enhancement and TEC perturbations, calculated in this publication, are only a function of the relative error that it is produced by the receiver noise that is less than 0.2 TEC units. The TEC values have been color coded according to the geographic latitude of the subionospheric intersection point as indicated in the color scale depicted in the lower right side of each frame. The TEC color coding has proved to be quite effective to identify the location of the equatorial anomaly and to study other processes that might produce a variation in latitude.

[10] Figure 2a shows the TEC daily variability in which TEC decreases after sunset and then increases near 06 LT as sunrise develops. In addition, there exists an anomalous TEC enhancement of ~10 units that lasts for several hours centered slightly before midnight when there is no EUV ion production. This resurgence of the TEC, dubbed here as the near-midnight TEC enhancement (N-MTECE), manifests as a sudden rise of the TEC values near 20 LT, a peak close to 23 LT, and a decay after 24 LT. The N-MTECE of Figure 2a displays a large latitudinal gradient as different TEC traces present colors varying from blue (8 TECu) to red (18 TECu). This is an increase of 10 TECu between the geographic latitudes of 18° S and 6° S. The TEC values of Figures 2b and 2c were obtained during the ascending phase of the present solar cycle and as a consequence show larger TEC values and much bigger N-MTECEs than the ones observed in 2008. In particular, the TEC enhancement seen on 11–12 March 2011 is the largest N-MTECE ever recorded in South America using GPS receivers. It is expected that as we move into the period of maximum activity of the present solar cycle, much larger TEC enhancements could be detected. The color scheme of the TEC values observed between 21 and 24 LT on 11 March 2011 indicates that the peak of the TEC enhancement occurs south of Huancayo and at a geographic latitude equal to 17° S. The N-MTECE of 21 March 2011 (Figure 2c) shows a rapid ascent of 25 TEC units without a clear latitudinal dependence. On this day the N-MTECE was observed by all low-latitude stations over South America. It is important to note when no N-MTECE develops, the TEC curves decrease almost linearly between 16 and 22 local time.

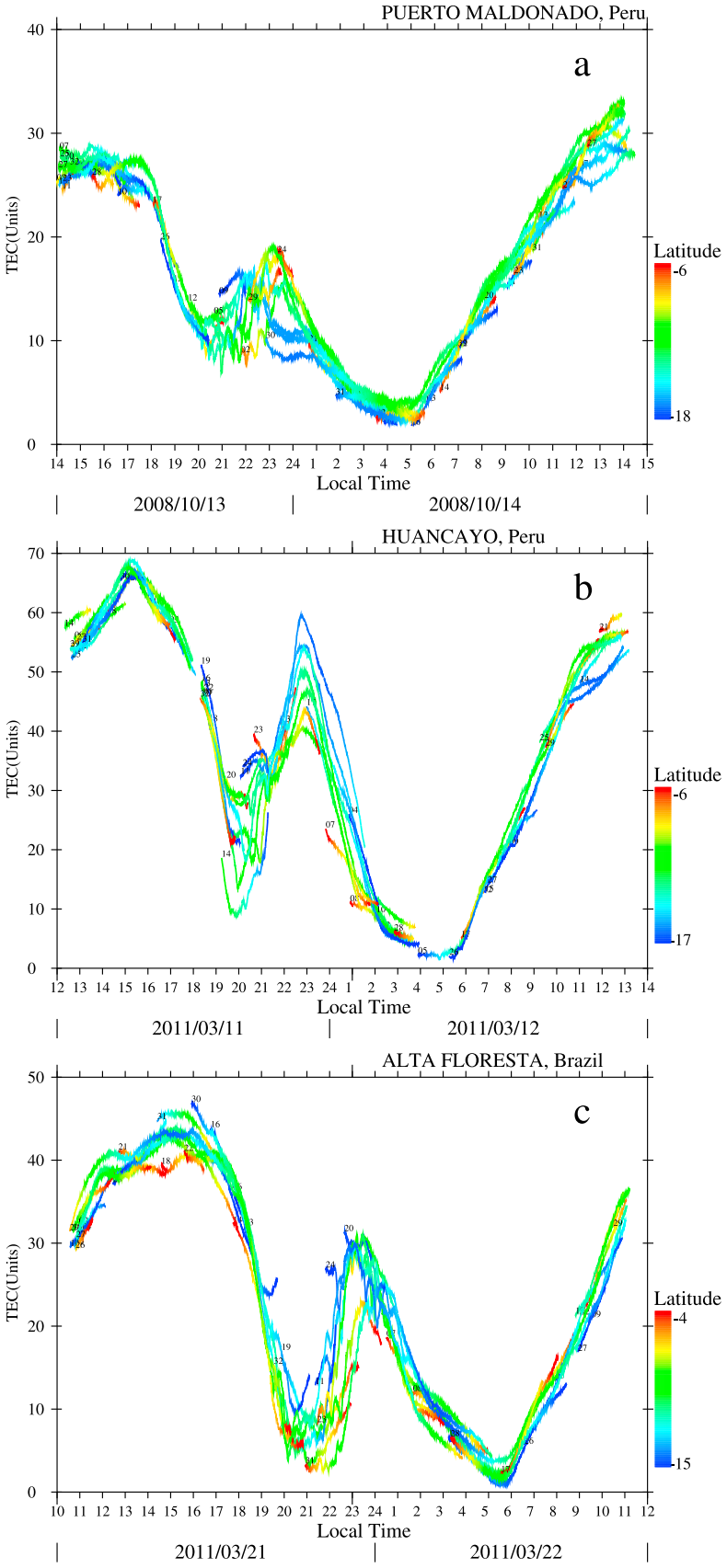
PUERTO MALDONADO, Peru
a
TEC(Units)
Latitude
-6
-18
Local Time
2008/10/13
2008/10/14
HUANCAYO, Peru
b
TEC(Units)
Latitude
-6
-17
Local Time
2011/03/11
2011/03/12
ALTA FLORESTA, Brazil
c
TEC(Units)
Latitude
-4
-15
Local Time
2011/03/21
2011/03/22

Figure 2

2.2. Regional Plots of TEC Corresponding to 14 October 2008

[11] Figure 3 introduces regional plots of TEC measured over the South American continent between 0030 and 0330 UT on 14 October 2008, a day of quiet magnetic conditions. On this day a 10 TECu N-MTECE was observed at Puerto Maldonado (Figure 2a). Figure 3a shows both crests of the equatorial anomaly extending between 60° and 80° W geographic longitude. Figures 3b and 3c, obtained 1 and 2 h after Figure 3a, indicate that the anomaly is receding and moving equatorward. This is a signature of the "reverse" fountain effect driven by a westward electric field in which the equatorial *F* region moves downward, producing pressure gradient forces along the field lines that can overcome gravity and cause the plasma to be transported upward along the field lines and toward the geomagnetic equator [*Sridharan et al.*, 1993; *Balan and Bailey*, 1995]. Figure 3d shows the region of maximum TEC placed at the boundary between Peru and Brazil (6° S, 72° W), or 6° north of the magnetic equator. The displacement between the region of maximum TEC and the magnetic equator is likely produced by a northward directed meridional wind that transports the plasma across the magnetic equator by reinforcing the plasma motion in the southern hemisphere and decreasing the plasma velocity in the northern side.

2.3. Regional Plots of TEC Corresponding to 12 March 2011

[12] Figure 4 shows the temporal variability of TEC measured over South America between 01 and 05 UT on 12 March 2011. Both 11 and 12 March 2011 were magnetically disturbed with a K_p value equal to 5^- at the time of the TEC enhancement. Each frame of Figure 4 shows the anomaly exhibiting a sharp longitudinal variability near 58° W. Similar sharp decrease was observed on 14 October 2008 (Figure 3). Figures 4b and 4c indicate that the crest of the anomaly decreases by 30 TEC units between 65° W and 50° W. The sequence of TEC images makes it evident that both crests of the anomaly move equatorward between 01 and 04 UT. Figure 4d indicates that the southern crest becomes more intense and outlives the northern crest. This effect is likely the result of a meridional wind that supplies plasma across the magnetic equator.

[13] To quantitatively assess the longitudinal and temporal variability of the anomaly, we have extracted TEC values along three latitudinal cuts parallel to the magnetic field lines that cross the magnetic equator at 70°, 60° and 50° W geographic longitude. Figure 5 shows the results of this analysis in which TEC is represented as a function of geographic latitude and universal times between 18 UT on 11 March 2011 and 06 UT on 12 March 2011. The horizontal white lines in each frame indicate the geographic latitude of the magnetic equator that varies from 12° S in Figure 5 (top) to 4° S in Figure 5 (bottom). We used the IGRF model containing coefficients for 2010 to calculate the position of the magnetic equator and the location of the field lines. Figure 5 confirms the existence of a prominent longitudinal variability of the anomaly and the TEC in general across South America. At 00 UT, it is observed that the TEC crests decrease from 60 TEC units in Figure 5 (top) to 40 TECu in Figure 5 (bottom). The maximum latitudinal separation of the anomaly, which occurs near 01 UT and almost simultaneously in all frames, is about 17°, 17° and 13° from top to bottom. The width of the crests of the anomaly also varies in longitude and it is wider in the western part of the continent. While the latter effect may be related to the larger number of GPS receivers along the eastern coast that provide much finer spatial resolution, the latitudinal displacement of the anomaly is mainly controlled by the electrodynamics of the nighttime *F* region ionosphere and it is likely related to a longitudinal difference in the vertical drift (zonal electric field).

2.4. Jicamarca Incoherent Scatter Radar Measurements on 11–12 March 2011

[14] Figure 6 shows density profiles measured by the Jicamarca incoherent scatter radar (ISR) on 11–12 March 2011. This figure displays the number density measured as a function of local time (5 h earlier than UT) and altitude. Coherent echoes were observed briefly in the *F* region bottomside between 19 and 21 LT and later at all altitudes between 04 and 06 LT. The development of coherent echoes is originated by the presence of 3 m scale structures associated with ESF that produce echoes 20 dB higher than the incoherent echoes [*Woodman and La Hoz*, 1976]. Figure 6 indicates that the F region elevates from a peak altitude of 400 km at 17 LT to above 600 km at 20 LT. The rise of the F layer [*Woodman*, 1970] and its subsequent lowering has been described by *Kudeki and Bhattacharyya* [1999] in terms of the prereversal enhancement (PRE) of the vertical drift and the postsunset vortex. During periods of an elevated *F* region or a significant PRE, it is common to measure ESF that obscures any attempt to measure the *F* region densities. However, during these observations no ESF echoes were observed between 2230 and 0400 LT, therefore, the Jicamarca ISR radar was able to detect the resurgence of the F region near midnight local time hours. In fact, the density over Jicamarca reached a value above 1.4×10^6 cm^{-3}. This value is higher than the peak density (10^6 cm^{-3}) observed at 17 LT. It is also significant that the density profiles between 2230 and 0030 LT show the *F* region peak descending in altitude. This observational feature is in agreement with the reverse fountain effect that is driven by a descending F region near the magnetic equator.

[15] The observations presented here consist of TEC values measured with the LISN GPS receivers (45) and several other networks of GPSs and density profiles measured with the Jicamarca radar. These data sets offer the possibility to diagnose the formation and decay of TEC enhancements in a regional scale. We have also shown that the TEC enhancements have a limited longitudinal extension, not more than 20° in longitude on 11–12 March 2011 and ~10° on 14 October 2008. It is also indicated that the

Figure 2. TEC values measured with 3 of the LISN GPS receivers on 3 different days. From the top to bottom, the TEC values for (a) Puerto Maldonado on 13–14 October 2008, (b) Huancayo on 11–12 March 2011, and (c) Alta Floresta on 21–22 March 2011. Note that the day is indicated at the bottom of each frame.

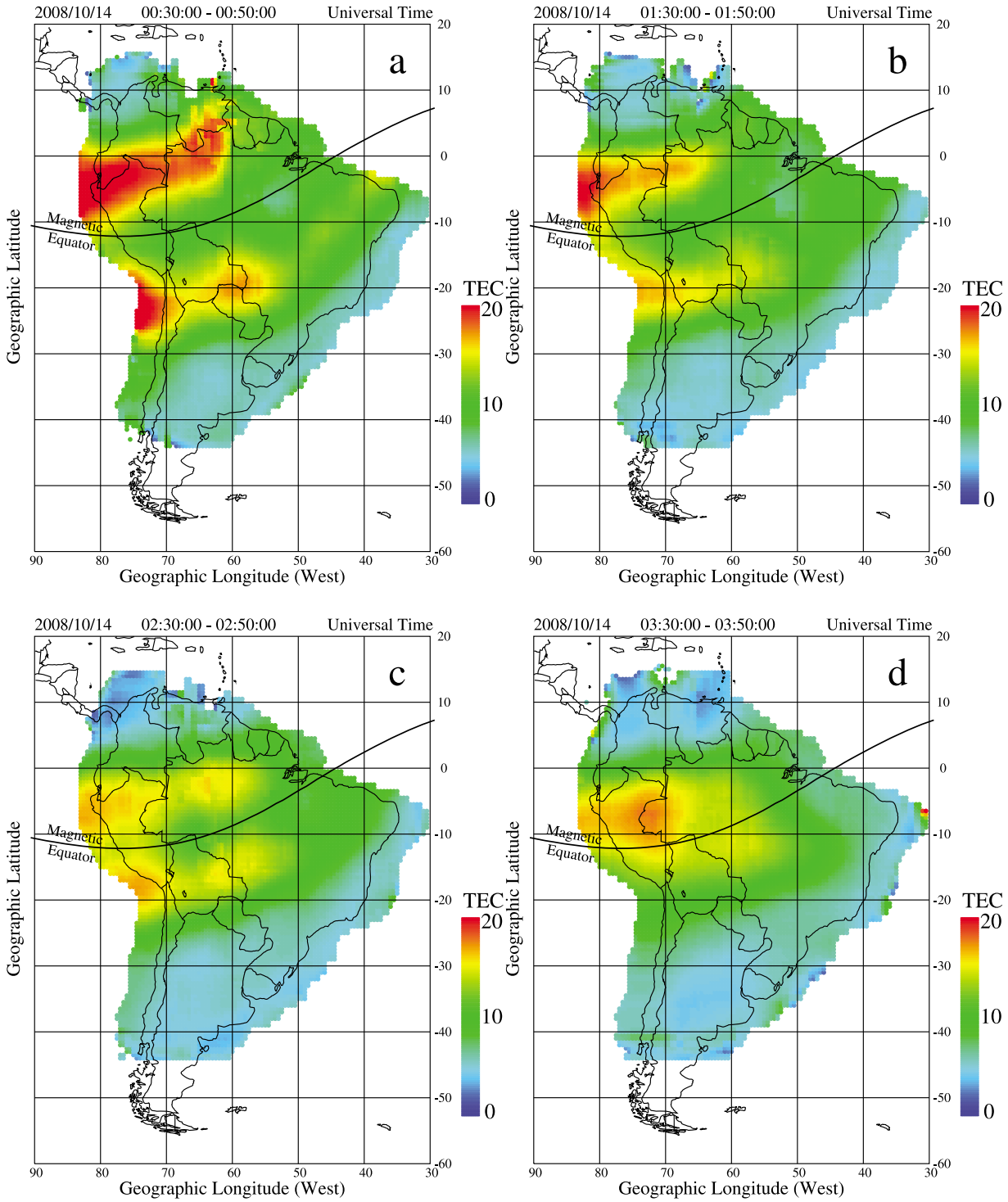

Figure 3. Regional maps of TEC values measured over South America between 0030 and 0330 UT on 14 October 2008. Note the evolution of the crests of the anomaly displacing equatorward and forming a single region of enhanced TEC that is located few degrees north of the magnetic equator.

existent GPS receivers over South America can indicate the locations where N-MTECE occur in a daily basis.

3. Detection of TIDs Using GPS Receivers

[16] The fact that TIDs produce fluctuations in the TEC values derived from beacon signals has made it possible to utilize small and/or regional arrays of GPS receivers to measure the characteristics of TID/GWs that propagate at high, middle, and low latitudes [*Afraimovich et al.*, 1998, 2003; *Ho et al.*, 1998; *Saito et al.*, 1998; *Shiokawa et al.*, 2002; *Valladares et al.*, 2009]. Observations [*Kirkland and Jacobson*, 1998] and model results [*Vadas*, 2007] have shown that most TIDs do not rise above 300 km. Thus, the

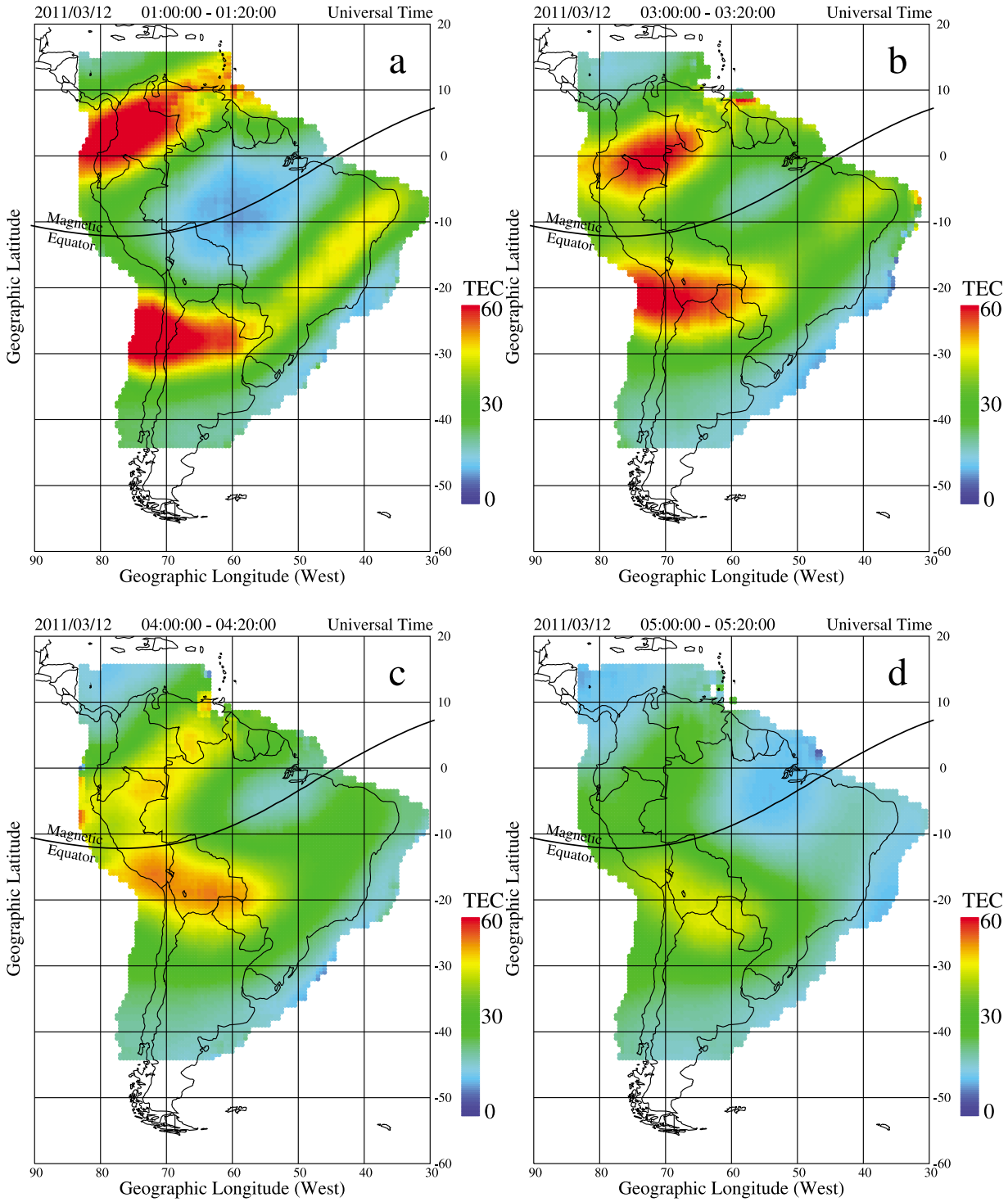

Figure 4. Same as Figure 3 but corresponding to 12 March 2011.

bulk of the TEC perturbations occur on the *F* region bottomside and the upper *E* region. In the radio-interferometry technique, phase differences measured at the various stations are used to determine TID velocity, propagation azimuth, and amplitude. Recently, the radio-interferometric technique has been adapted for use with GPS satellites [*Afraimovich et al.*, 1998, 2000, 2003]. This new innovation makes it possible to utilize inexpensive, easily deployed GPS receivers to study gravity waves at a wide variety of locations. The large number of GPS satellites in orbit makes it possible to continuously monitor the bottomside region over a given receiver array.

[17] *Valladares and Hei* [2012] have recently used a GPS-radio interferometer (GPS-RI) to measure the phase velocity

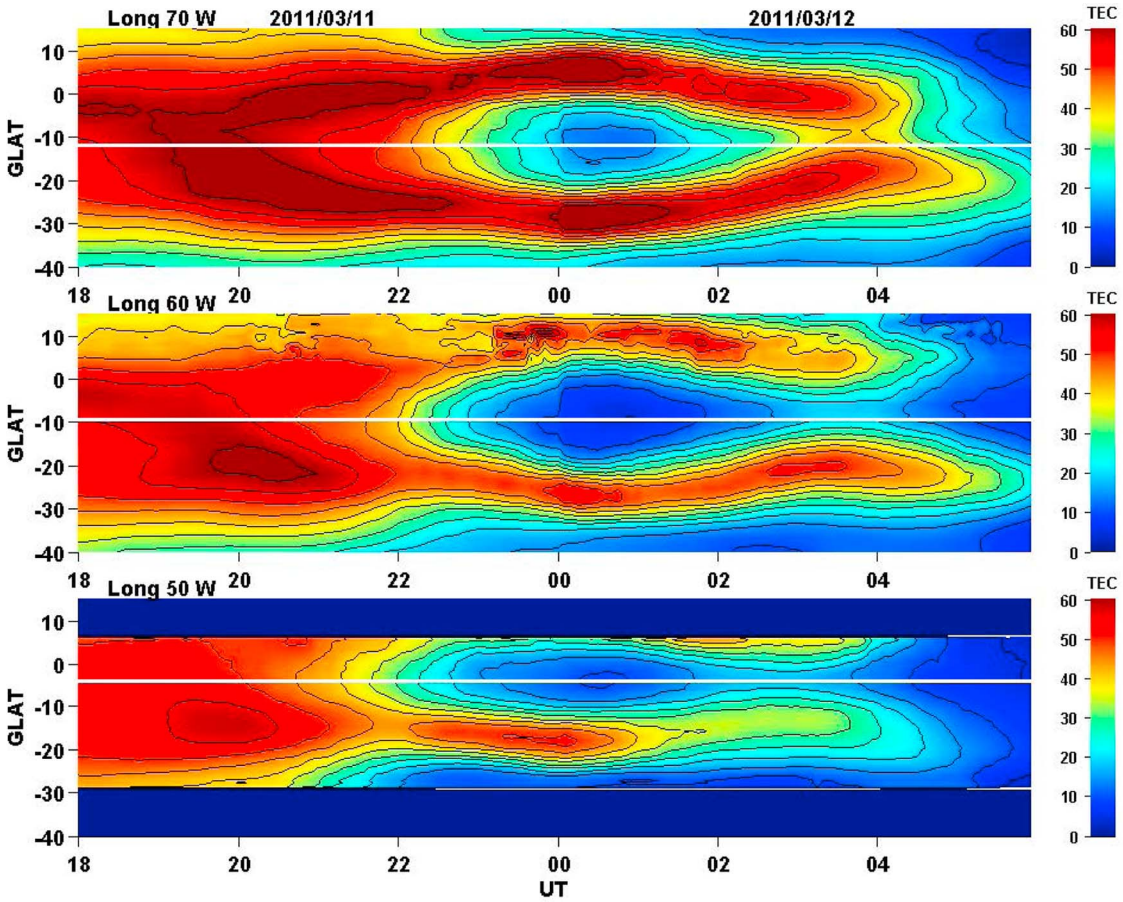

Figure 5. TEC values along three latitudinal sections parallel to the magnetic field lines within the South American continent. The magnetic field lines intersect the magnetic equator at 70°, 60°, and 50°W geographic longitude. Note the variability of TEC as a function of time and longitude.

and propagation direction of gravity waves that were circulating near Huancayo (12.042° S, 75.321° W) in Peru. A small array of three GPS receivers separated by 4–5 km was implemented near Huancayo by adding two more GPS receivers and placing them at the vertices of an equilateral triangle. The phase velocity and direction of propagation was extracted by using two algorithms: the Statistical Angle of Arrival and Doppler Method for GPS interferometry (SADM-GPS) and the cross-correlation method (CCM). Both methods agreed that on 20 July 2008 between 22 and 24 UT several TIDs moved across the small array of GPS receivers with a velocity near 130 m/s, were directed northward and had wavelengths close to 450 km. The CCM method was also applied to TEC values collected by other LISN GPS receivers that were operating hundreds of km away from Huancayo. Figure 7 shows the results of CCM method applied to GPS stations separated by hundreds of km in which the magnitude and direction of the TID phase velocity are represented by arrows. The size of the arrow is proportional to the phase velocity of the GW, and the azimuthal angle of the arrow is a function of the propagation direction. In this scheme, an arrow pointing to the top indicates a northward propagation direction. Regardless the large distances between receivers, the coherence of the TEC traces was high and a phase velocity equal to 150 m/s and a northward propagation direction were obtained using the GPS at Piura (5.170° S, 80.639° W), Cuzco (13.520° S, 71.959° W) and Huancayo.

[18] Figure 8 presents the TEC perturbations (TECP) for all 126 GPS receivers that operated in South America on 20 July 2008. The simultaneous operation of these GPS receivers provides good coverage over the South American continent, except for latitudes southward of 40° S. The TECP values are plotted in red, centered along the satellite trajectory (thin black line), containing amplitudes higher than 0.4 TEC units. This baseline value is about 4 times higher than the noise level of TEC fluctuations. The sequence of regional plots in Figure 8 demonstrates that TIDs were mainly restricted to the western side of South America between 1900 and 2200 UT. Figures 8a–8c show that TECPs originated in the northern part of Chile (Lat = 25° S) and traveled northward in agreement with the velocity calculations presented in Figure 7. Note that the displacement of the TECP signatures from 25° S to 15° S in 2 h implies a velocity equal to 154 m/s. This is also in agreement with the GW velocity determined using three stations in Peru (Figure 7).

3.1. TIDs Observed on 17 July 2008

[19] Figure 9 shows TECP values measured at Iquitos (3.77° S, 73.27° W), Piura (5.17° S, 80.64° W) Huancayo, and Cuzco on 17 July 2008. We have defined the TECP

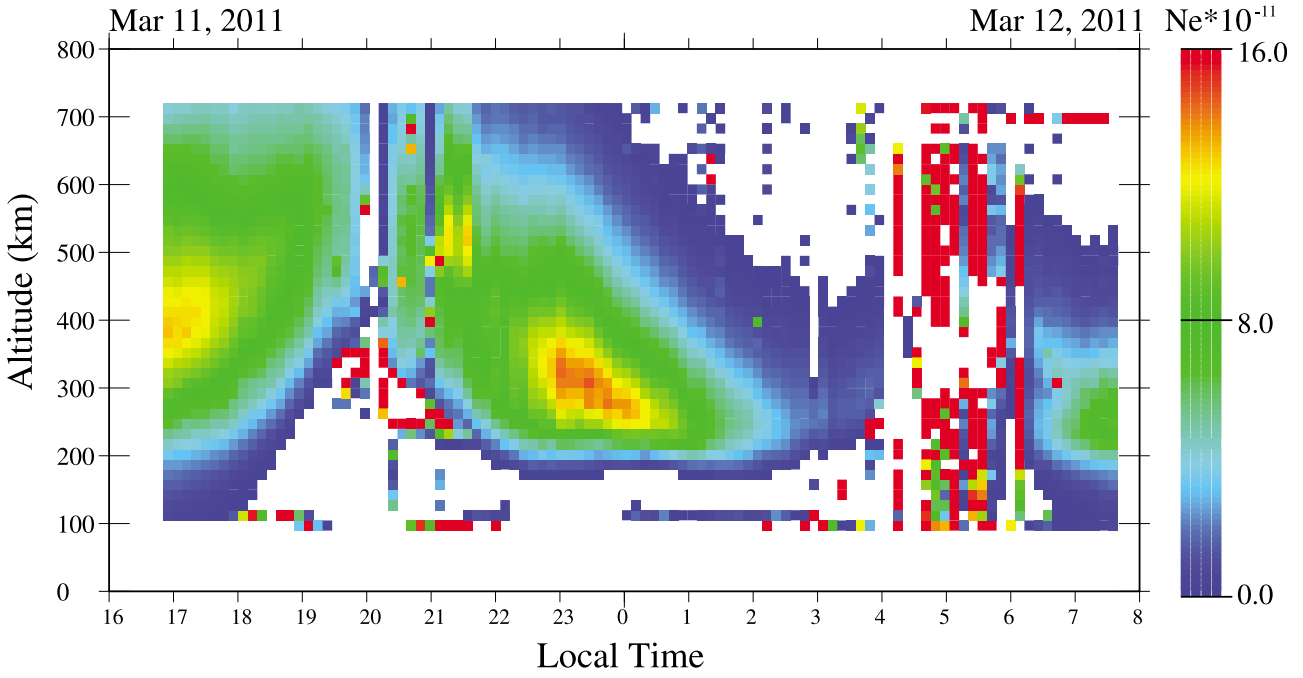

Figure 6. Density profiles measured by the Jicamarca ISR on 11 and 12 March 2011. Incoherent echoes were obtained mainly between 1700 and 0400 LT. There is a patch of coherent echoes extending to all altitudes between 0400 and 0615 LT.

values as the difference between the measured TEC and the estimated background or "unperturbed" TEC values. The unperturbed TEC values were calculated fitting a fourth-order polynomial function to every 3 h segment of TEC values. This procedure filters out geophysical effects that commonly have a temporal resolution of a few hours and waves with periodicities larger than 3 h. We also removed high-frequency noise effects using a band pass filter with a cutoff frequency set at 5 min. In addition, the observations presented here correspond to local times and seasons when no TEC depletions commonly develop. Therefore, the TEC perturbation defined here are likely associated with density variations produced by the passage of the gravity waves. The Huancayo and Cuzco stations are located close to the magnetic equator. Note that TECP values for Huancayo have a 1 s temporal resolution compared to 10 s for Iquitos, Piura, and Cuzco. All four stations display TECP values reaching 1 or more TECu between 20 and 22 UT. TEC perturbations containing smaller amplitudes (±0.4 TECu) are observed between 13 and 19 UT at all four receivers.

3.2. Analysis of TID Characteristics Observed on 17 July 2008

[20] The phase velocity ($V_h(t)$), and the direction of propagation ($\alpha(t)$) of the TIDs were calculated using the cross-correlation method (CCM) described by *Valladares and Hei* [2012]. These authors indicated that the velocity and angle of propagation of the TIDs can be calculated by using TECP values from a small network of three GPS receivers, even if the receiver separation is of order hundreds of kms. One receiver acts as the reference point and its location defines the center of the coordinate system. TECP values of this receiver are correlated with the values corresponding to the other two receivers, therefore, deriving the time offset along two different baselines. These time offsets and the following equations are used to resolve both components of the phase velocity.

$$\alpha(t) = \arctan((Y_A T_{B-C} - Y_C T_{B-A})/(X_C T_{B-A} - X_A T_{B-C})) \quad (1)$$

$$Vh(t) = (Y_C \cos(\alpha(t)) + X_C \sin(\alpha(t)))/T_{B-C} + w_x(t) \sin\alpha(t) + w_y(t) \cos\alpha(t) \quad (2)$$

$T_{B\text{-}A}$ and $T_{B\text{-}C}$ are the time delays between the TECP traces. The symbols X_A, Y_A, X_C, and Y_C correspond to the distances between both additional GPS receivers and the center receiver in a Cartesian coordinate system. $w_x(t)$, and $w_y(t)$ are the velocities of the x and y projections of the subionospheric intersection point. In this analysis, we have assigned Huancayo to be the reference receiver (also called B). Nevertheless, any receiver of the subnetwork can act as the center receiver.

[21] Figure 10 shows the results of the CCM method based on signals from the PRN 32 GPS satellite recorded at

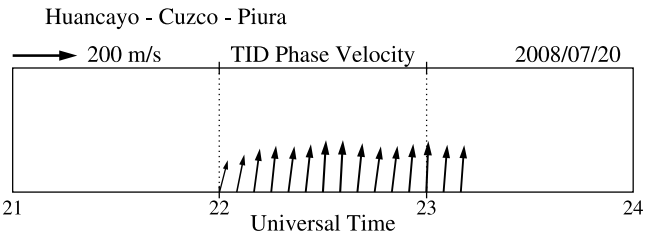

Figure 7. Phase velocities of the TIDs calculated using the CCM method and TEC perturbation values from Huancayo, Cuzco, and Piura for 20 July 2008.

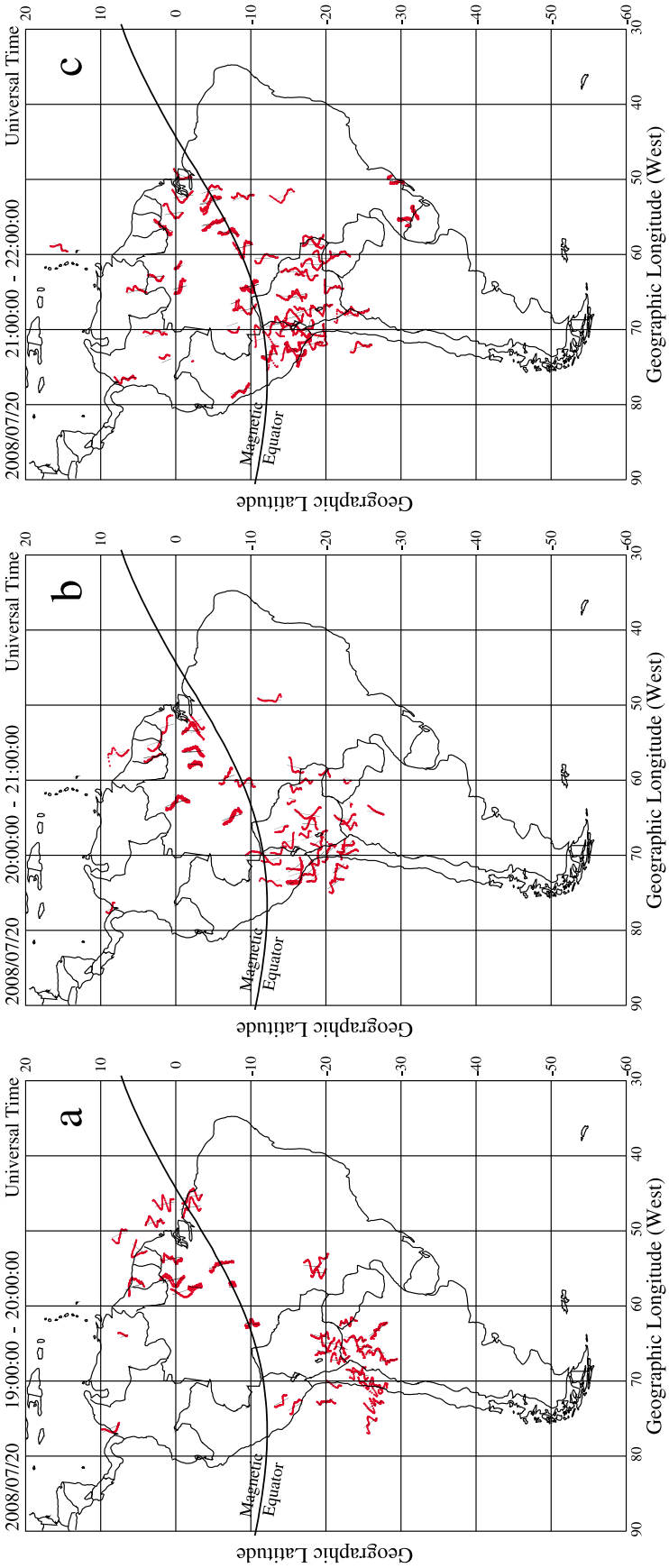

Figure 8. Temporal evolution of TEC perturbations recorded by several GPS sites that operated in South America on 20 July 2008. The red traces correspond to the TECP values after subtracting the daily variability.

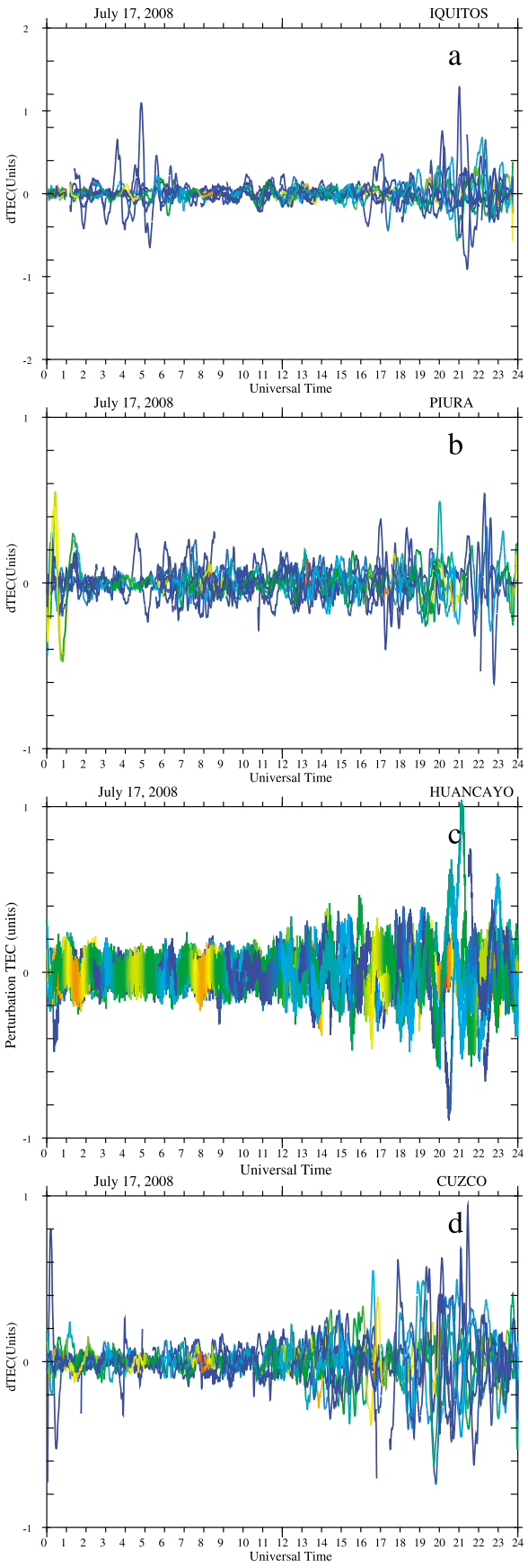

Huancayo, Iquitos and Cuzco. Figure 10 (bottom) displays the TECP values for Huancayo (in blue), Cuzco (Figure 10, bottom left, in red) and Iquitos (Figure 10, bottom right, in red). Figure 10 (top left) presents the CCFs calculated using the Huancayo and Cuzco TECPs showing a time delay that varies from −10 min at 19 UT to +3 min at 23 UT. Note that a negative (positive) offset is an indication that Huancayo's TECP lags (leads) Cuzco's. This is evident in Figure 10 (bottom left) in which the red trace (Cuzco) leads the blue trace (Huancayo) for few minutes. Figure 10 (top right) displays CCFs for Huancayo and Iquitos. The time delay for these two stations varies between −50 min at 19 UT and −37 min at 22 UT. Based on the timing relationship for all three stations, it can be concluded that the TEC perturbation was seen first at Iquitos, located further north, then at Cuzco and later at Huancayo (the latter two are placed near the magnetic equator) implying a direction of motion toward the southeast (see Figure 11). Figure 10 (top right) also shows a secondary peak containing amplitudes slightly smaller, but placed ∼75 min away from the primary maximum. We believe that the secondary maximum is produced at multiples of the scale size of the TID (∼75 min). *Afraimovich et al.* [2003] reported that quite often a series of quasi-sinusoidal variations in TECP are observed at midlatitudes. They termed these features traveling wave packets. We are also observing traveling wave packets in South America; the secondary maximum is due to the repetitive nature of the TIDs. It is also pointed out that the CCF amplitude scale was limited to values above 0.4 and did not include negative values as they would indicate anticorrelations. If we had used a CCF amplitude scale varying between −1 and 1, a negative peak would have been observed between the primary and secondary maxima. It is also indicated that the CCM method employs TECP values recorded from the same GPS satellite due to the motion of the satellite that produces almost the same temporal delay on receivers placed at relatively close distances. This satellite motion effect can be removed after we calculate the phase velocity. If signals from different GPS satellites were used, it would be necessary to remove the effect of the satellite motion before the CCF is calculated. We have also used TECP values from Leticia (not shown here) to verify that the propagation direction of the TIDs was in the southwest direction on 17 July 2008 and between 18 and 22 UT. As the distance between Iquitos and Leticia is about 350 km (see Figure 11), it was determined that the Leticia TECP trace was leading the corresponding values from Iquitos.

[22] The phase velocity and the angle of propagation was calculated using TECP traces from all four stations presented in Figure 9, but forming two sets of three receivers each. The first set consisted of the receivers at Huancayo, Cuzco and Iquitos. The other set of three receivers was formed with the Huancayo, Cuzco and Piura GPS receivers. The CCM method was applied to signals from all the GPS satellites that had a line of sight above 35° elevation. Cross correlations functions similar to Figure 10 were obtained for PRNs

Figure 9. TEC perturbations measured at Iquitos, Piura, Huancayo, and Cuzco on 17 July 2008. Data from various GPS satellite signals are plotted; each satellite is distinguished by a different color. Note the TECP values near or above 1 TECu between 20 and 21 UT.

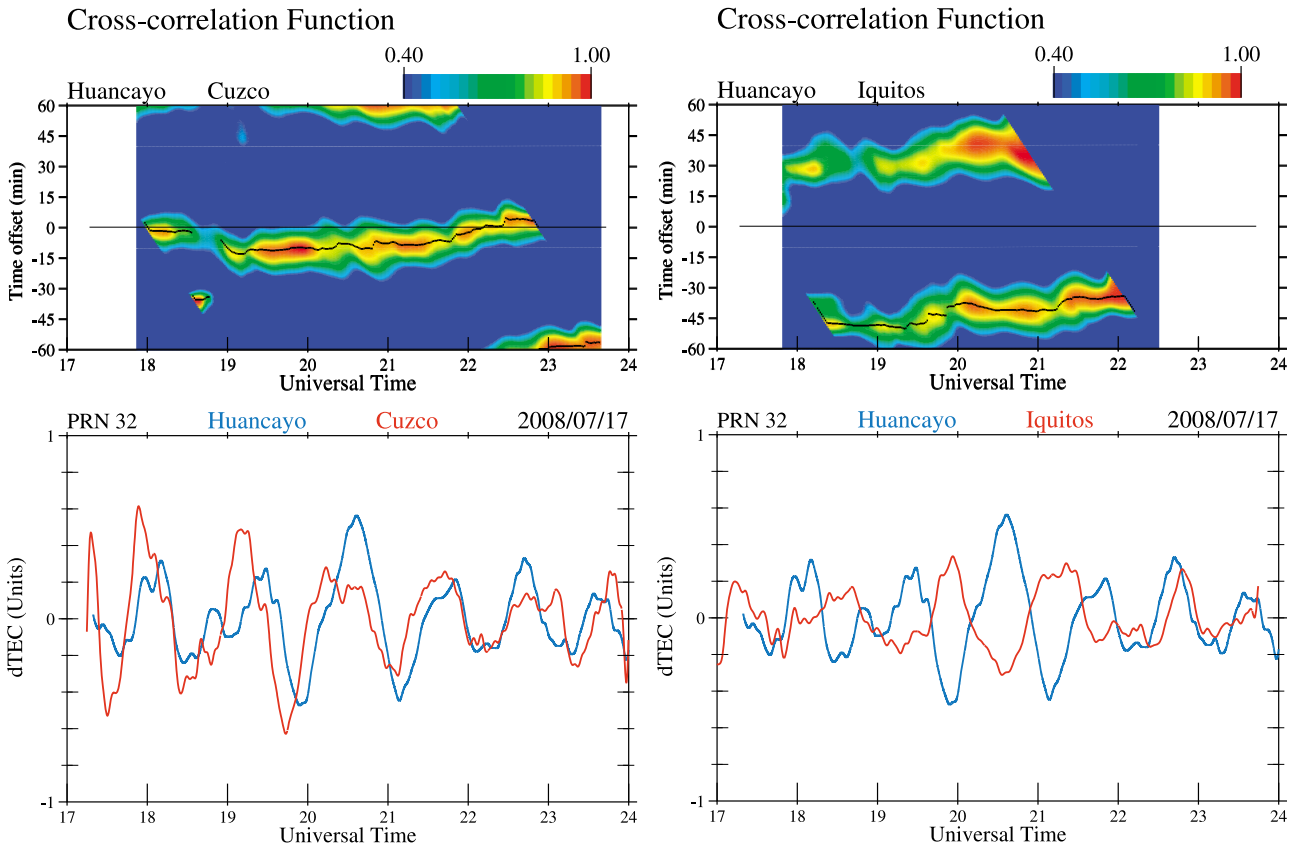

Figure 10. (top) Cross correlation functions and (bottom) TECP curves for GPS satellite 32. (left) The CCFs for TECP signals from Huancayo and Cuzco. (right) Huancayo and Iquitos. The cross-correlation functions are plotted using a color scale that varies between 0.4 and 1.0. The black line that crosses near the middle in Figure 10 (top left) corresponds to the correlation maximum and it is taken as the time delay (T_{B-A} or T_{B-C}).

03, 20, and 23. Figure 11 shows the location of four GPS receivers in Peru (large red dots) that were used to calculate the characteristics of the TIDs. Also plotted are the subionospheric intersection points for PRN 32. The black dots placed over the colored lines indicate the location of the subionospheric intersection points at the hour every hour. Note that the subionospheric intersection paths are closely parallel for all 4 traces.

[23] Figure 12 shows the average velocity and direction of propagation of the TIDs measured with two sets of three GPS receivers each, using a total of four dual-frequency GPS receivers. The amplitude of the TID's velocity varies between 250 m/s and 190 m/s at 19 and 22 UT, respectively. The angle of propagation of the TIDs was toward the southwest direction ($-140°$ from geographic north). At earlier and later times the amplitude of the TECP values was much smaller and no reasonable TID velocities were obtained. Other GPS receivers in Peru and the neighboring countries also detected the TIDs during this event.

4. Detection of TEC Depletions Using GPS Receivers

[24] We mentioned above that the LISN community is presently managing the operations of 45 dual-frequency GPS receivers in South America. These GPSs and the ever-growing number of receivers dedicated to study geodynamics have created a formidable observing platform to diagnose the characteristics of plasma depletions over South America. The main advantages of this system are the spatial coverage of the probing volume that extends over the continent, the continuity of the observations, and the low cost of the instrument, its deployment, and the day-to-day routine operations. Due to the sudden and deep decrease in the TEC values that the bubbles produce, several authors have used GPS measurements to investigate the characteristics of plasma bubbles. [*Valladares et al.*, 2004; *Conker et al.*, 2004; *Rama Rao et al.*, 2006; and *Portillo et al.*, 2008]. Recently, *Seemala and Valladares* [2011] have presented a new algorithm that can be used to detect the existence of TEC depletions in the TEC data measured with the GPS receivers that operate in South America. This algorithm has been used to automatically detect TEC depletions and study their characteristics during two years of low solar activity: 2008 and 2009.

[25] Figure 13 shows the TEC depletions detected over South America on 2 consecutive days: 13 and 14 March 2008. The color segments correspond to the geographic locations of the start and end points of the TEC depletions identified from each satellite pass and for each receiver. The

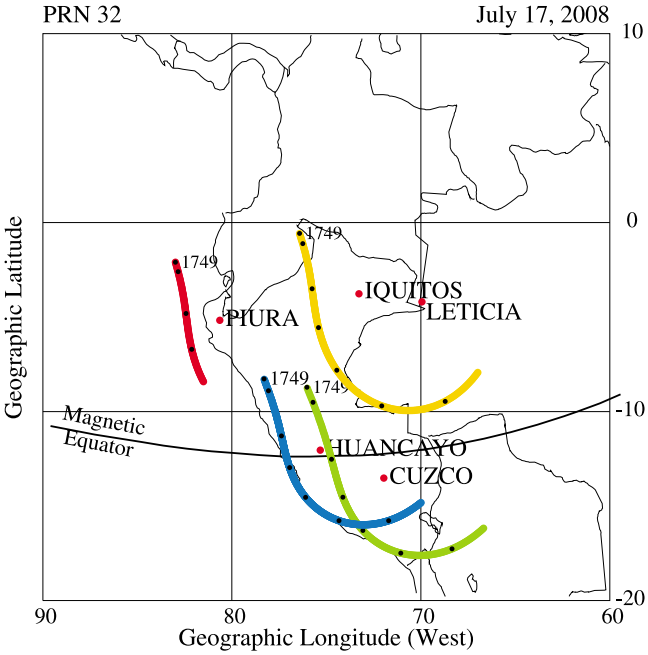

Figure 11. Subionospheric intersection points of the trajectory of the GPS satellite 32. Note the location of the four stations that contributed with TEC values to calculate the TID phase velocities. The intersection points are closely parallel.

color coding indicates the universal time when the depletions were detected, according to the numbers indicated at the top of each frame. It is quite likely that any single depletion or plasma bubble was observed simultaneously by one or more receivers at different latitudes. Therefore, the number of TEC depletion detections is a function of the number of receivers and certainly more than the number of plasma bubbles in the region. The slow east–west motion of the GPS satellites and the nature of the passes that is mainly in the north–south direction, are quite favorable to measure the east–west extension of the plasma depletions. On 13 March TEC depletions are seen only at the center of South America (between 70° W and 55° W). On 14 March 2008, TEC depletions occur only in the western and eastern sides of the continent. In addition, the majority of the TEC depletions observed on 14 March 2008 in the western side are colored red, meaning that they were recorded between 04 and 09 UT (close to and after midnight). These two plots display the large day-to-day variability of the depletion distribution over South America. *Seemala and Valladares* [2011] pointed out that in spite of the prominent daily variability, the climatology of the TEC depletions follows the longitudinal characteristics of plasma bubbles presented by other authors [*Huang et al.*, 2001; *Burke et al.*, 2004] and Tsunoda's hypothesis that plasma bubble activity increases when the solar terminator aligns with the geomagnetic field [*Tsunoda*, 1985].

[26] We have constructed maps of TEC depletions similar to Figure 13 for each day of years 2008 and 2009 and recorded the number of depletion detections for each day. The result of this analysis is presented in Figure 14 in which the number of detections is displayed as a function of local time and month of the year. Figure 14a displays the statistics of TEC depletions for year 2008 and Figure 14b shows similar results for 2009. Both frames show the typical seasonality of plasma bubbles over South America that consists of a broad maximum extending between October and March and a minimum or a null number of depletions between the months of May and August. The variability of the Earth's magnetic field declination across South America produces an equinoctial maximum of plasma bubbles near the west coast and a December solstice peak on the eastern side. As Figure 14 includes all the depletions detected over the continent, both local maxima unify in a broad peak extending for several months. Two important features observed in Figure 14 consist of (1) the later bubble onset time during the months of April, August and part of September and (2) the multiday periodic variation of the number of bubble detections during the time of peak occurrence of TEC depletions, say 22 LT. The latter effect is more evident during the months of January, February and March in 2008 and October, November and December in 2009. This period is approximately 28 days and probably associated with lunar tide effects. The late local time appearance of TEC depletions between April and September may be associated with a slow initiation of the depletions during these months as the PRE decreases in magnitude in this longitudinal sector [*Fejer et al.*, 2008; *Pacheco et al.*, 2010] or a later appearance of the seeds.

5. Discussion

5.1. On the Near-Midnight TEC Enhancements

[27] We have presented a detailed description of the temporal evolution and the spatial extension of the N-MTECE that were observed at low latitudes during both magnetically quiet and disturbed conditions. The TEC enhancements that were measured with the LISN and other networks of GPS receivers operating in South American occurred quite often during years of low solar activity. They are expected to appear equally frequently during other phases of the solar cycle. *Balan and Rao* [1984] described the characteristics of TEC enhancements observed in India using signals from the ATS 6 satellite. These authors reported that the intensity and duration of the TEC enhancements are maximum at equinox and minimum in summer. Later, *Balan and Bailey* [1995] used the Sheffield University plasmasphere-ionosphere model (SUPIM) to investigate the importance of diffusion, E × B drifts and neutral winds on the fountain effect and the formation of an additional layer (called the G or F3 layer). It was reported that after sunset and soon after the drift turns downward, the fountain becomes a reverse fountain in which the supply of ionization is not from the equatorial zone but

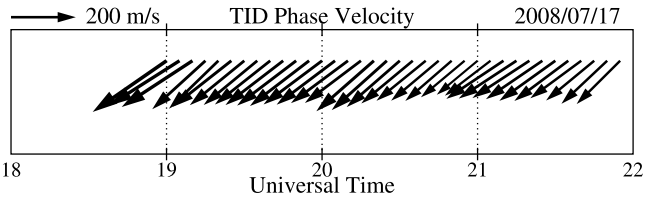

Figure 12. Same as Figure 7 but for TIDs phase velocities measured on 17 July 2008 using TEC values from Iquitos, Piura, Huancayo, and Cuzco.

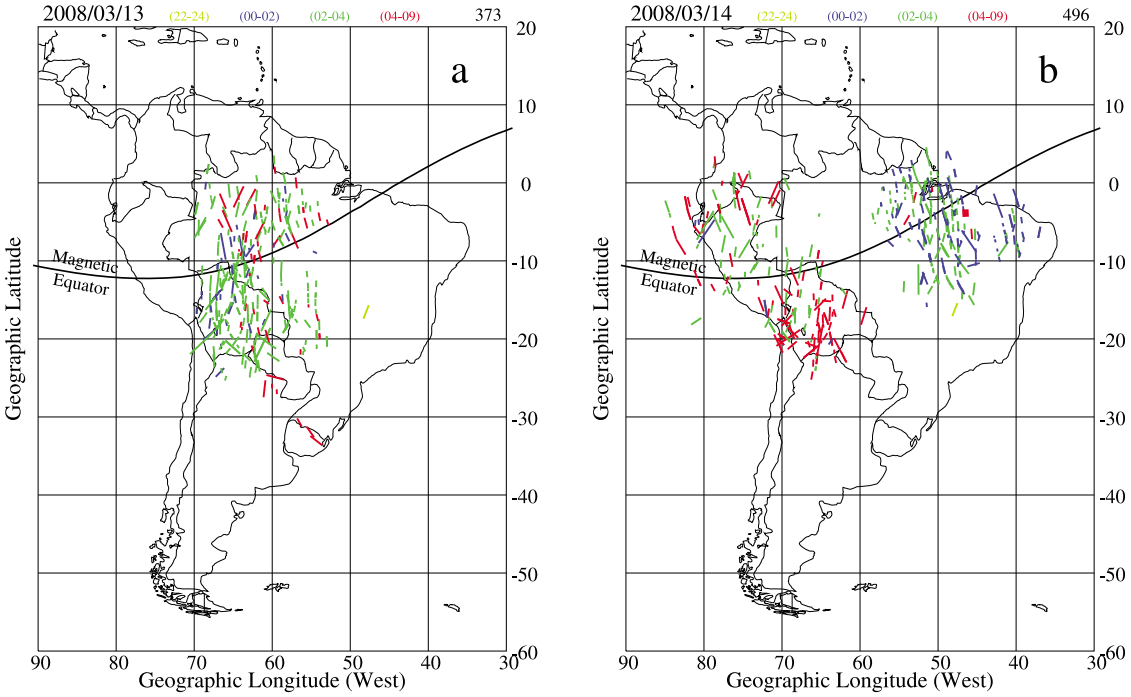

Figure 13. TEC depletions detected from all GPS receivers over the South American continent on (a) 13 March 2008 and (b) 14 March 2008. These two events exemplify the large day-to-day variability that exists in the distribution of TEC depletions over South America.

from the anomaly region. *Balan and Bailey* [1995] demonstrated that the reverse fountain acts as the main source for the nighttime increase in ionization at low-latitude stations. Figure 5 has shown that the N-MTECE is part of the equatorial anomaly that recedes and displaces toward the equator after sunset. It is indicated here that the anomaly displacement is driven by the reverse fountain effect and a downward E × B drift. Figures 3 and 4 indicated that the final location of the region of enhanced TEC was not at the magnetic equator, but displaced few degrees to the north or south. *Balan and Bailey* [1995] stated that the neutral wind acts as a modulating source and makes the anomaly asymmetric. We believe that the final latitude of the N-MTECE region is associated with the magnitude and direction of the meridional wind that makes one crest contain more ionization than the other crest.

[28] A unique database has been accumulated to define and characterize the TEC enhancement of 11–12 March 2011. TEC values measured by more than 200 GPS receivers in South America, density profiles gathered with the Jicamarca ISR and other ancillary data sets offer the possibility to conduct data assimilation to calculate zonal electric fields and meridional neutral winds. The data assimilation and modeling work will be presented and discussed in a future publication.

[29] The regional coverage of our measurements has revealed that the region of N-MTECE did not extend more that 10° in longitude on 14 October 2008 and no more than 20° on 12 March 2011. This limited longitudinal extension is not related to the difference in local time between different sectors in South America, nor the prominent variability of the magnetic field across South America, but likely to the longitudinal variability of the electric field (and fountain effects) in different parts of the continent. The three events presented here developed in the western part of South America; however, we have also observed N-MTECE at the center and eastern parts of South America.

5.2. On the Detection of TIDs Using Networks of GPS Receivers

[30] We have applied the CCM method to analyze TECP values collected by several GPS receivers that belong to the LISN network and are operating at Ancon, Huancayo, Piura, Cuzco, Iquitos and Leticia. We found very good correlation, in excess of 0.9, between the TECP traces corresponding to stations placed hundreds of kms away. We were able to calculate that the angle of propagation $\alpha(t)$ was close to $-140°$ (southwestward propagation) and the horizontal phase velocity, $V_h(t)$ was between 190 and 250 m/s. The characteristics of the phase velocity measured on 17 July 2008 are quite different to the velocity of the TIDs measured on 20 July 2008 that were reported by *Valladares and Hei* [2012]. We believe that these differences are attributed to the day-to-day variability of the TIDs over South America.

[31] It has been shown that the existence of over 200 GPS receivers in South America and the large traveling distance of the TIDs offer the possibility of combining measurements of TEC perturbations from adjacent receivers to obtain the velocity of TIDs, their direction of motion and their wavelengths. Nevertheless, it is noted that several geometrical considerations need to be accounted for with more precision. One of them is the fact that the projection of the apparent satellite motion over the propagation direction of the TID may vary during the travel time between the LISN stations. It is also possible that the TID wavefront may have a circular

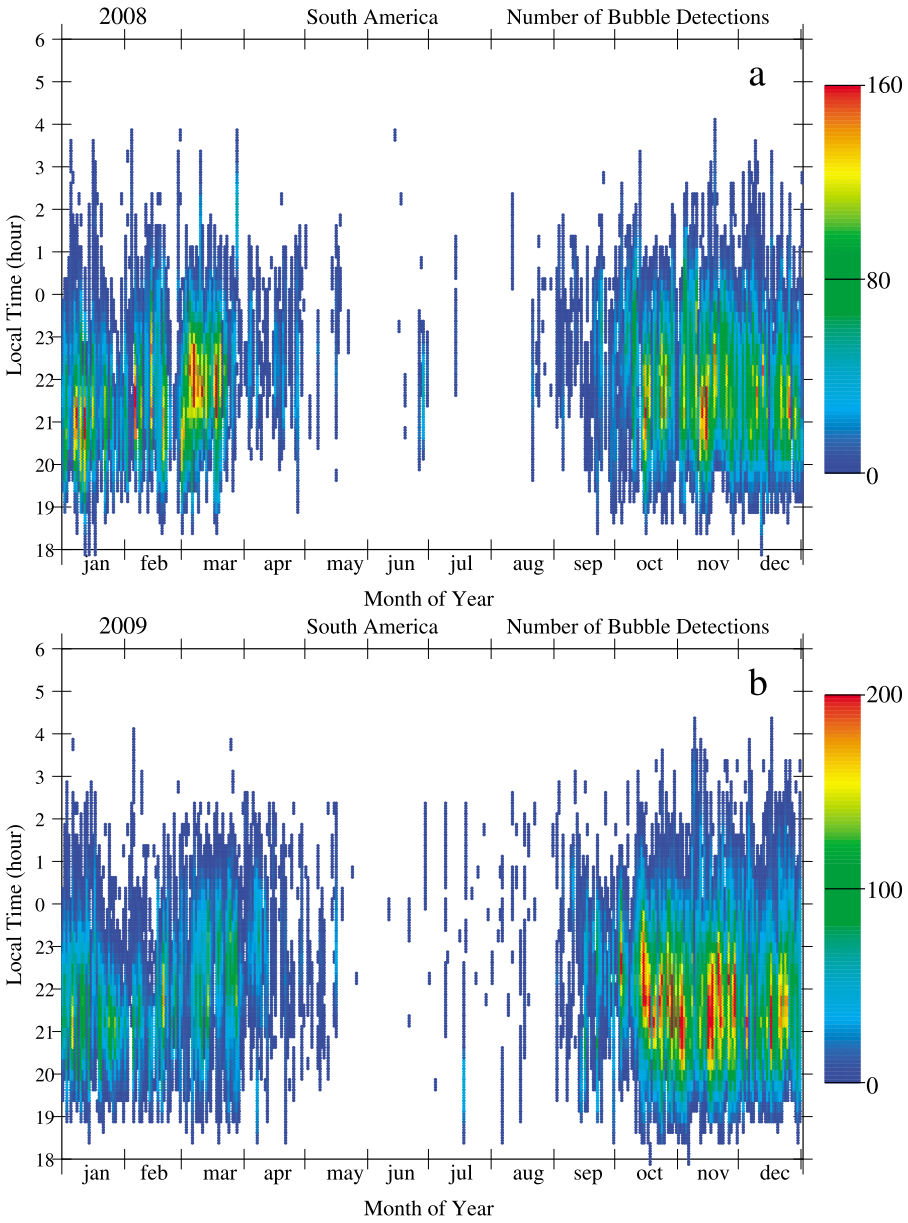

Figure 14. Total number of bubble detections observed over South America for every day of 2008 and 2009. Note the periodicity (~28 days) seen in the early months of 2008 and the late part of 2009.

shape. The GPS radio-interferometry method that was used here is one of the most effective techniques with which to observe GW/TID activity at low latitudes.

[32] Low-latitude TIDs are important to study because they are a key mechanism by which energy and momentum are deposited into the thermosphere. Moreover, TIDs are thought to be a key seed mechanism of plasma depletions. While evidence of TID seeding was found during the Spread-FEx campaigns [*Fritts et al.*, 2008], never before has it been possible to continuously monitor TID activity on the *F* region bottomside during the crucial early evening hours, when seeding occurs. The GPS receivers that presently exists in South America used as radio-interferometers and the analysis described here opens the possibility of locating and characterizing TIDs during times when seeding occurs.

5.3. On the Detection of TEC Depletions Using Networks of GPS Receivers

[33] An earlier publication has presented regional plots of TEC depletions observed across the South American continent [*Seemala and Valladares*, 2011] and introduced the dramatic day-to-day variability of depletions for a year of low solar activity: 2008. Figure 13 has also shown that TEC depletions can occur in limited regions of the continent containing a day-to-day variability with no apparent ordered patterns.

[34] *Aarons* [1993] and *Huang et al.* [2001] have shown that the occurrence characteristics of plasma depletions depend strongly on season and longitude. To explain the climatology, *Tsunoda* [1985] introduced the hypothesis that ESF activity increases when the solar terminator aligns with

the geomagnetic field. The solar terminator B alignment (STBA) hypothesis states that the occurrence frequency of equatorial plasma depletions will be higher during the equinoxes in the Peruvian sector, where the field lines are mainly north–south, and also high during the December solstice in Brazil where the magnetic declination is largely westward. In addition to the seasonal climatology, *Seemala and Valladares* [2011] showed that there exist days in the equinoxes as well as in the December solstice when the depletions are seen at all longitudes or are observed in regions that do not agree with the STBA hypothesis.

[35] We believe that to explain the day-to-day variability, it is necessary to consider the role that seeds may have to initiate the Rayleigh-Taylor instability. It has been suggested that perturbations in the neutral gas such as gravity waves stimulate a response in plasma density only when there is alignment in the phase fronts of GWs with the magnetic field $\boldsymbol{B}$ lines [*Huang and Kelley*, 1996; *Tsunoda*, 2010a]. We have demonstrated in this report that the LISN network of GPS receivers can be used to diagnose the presence of GWs and calculate their phase velocity and propagation direction. This fact speaks out of the advantage of the LISN observatory to resolve the role of GWs on seeding equatorial plasma bubbles. It is suggested here that the occurrence of TEC depletions in regions of the South America continent where the local ionospheric conditions are not favorable for the STBA hypothesis, can be understood if the number and amplitude of the GWs is large enough to seed plasma bubbles and overcome stable conditions.

[36] It has been suggested that eastward neutral winds in regions of westward plasma flows, as happens at the bottom of the *F* region right after sunset, can generate the proper conditions for bubbles to develop [*Kudeki et al.*, 2007]. The eastward zonal winds are responsible for the prereversal enhancement of the vertical velocities and the consequent uplift of the F layer to the more unstable higher altitudes. They can also drive 10s of km scale density waves with wavefronts tilted 45° to the west during the initial phase of the postsunset vortex [*Kudeki et al.*, 2007]. These waves can act as the seeds for the larger-scale plasma bubbles. It is indicated that a database of zonal winds measured by the existent Fabry-Perot instruments that are presently operating in the continent will help to determine the role of the neutral winds on plasma bubble seeding.

5.4. Studies of the Low-Latitude Ionosphere-Thermosphere System Using the LISN Observatory

[37] As indicated in the introduction, the LISN distributed observatory has a network of 5 magnetometers forming 2 baselines that can provide daytime electric fields at 2 different longitudes. Preliminary results based on magnetic field measurements have been reported elsewhere (E. Yizengaw et al., Longitudinal differences of Ionospheric vertical density distribution and equatorial electrodynamics, submitted to *Journal of Geophysical Research*, 2011) and comparison with similar networks in Africa are underway. The network of VIPIR ionosondes is under deployment including 4 new VIPIRs to be installed in 2012. It is suggested that the new instrumentation together with the analysis techniques described in this report will help us to (1) understand the physics of the day-to-day variability of the low-latitude ionosphere and then (2) devise a method to predict the initiation and development of the ESF irregularities. More specifically, we plan to develop numerical methods that will provide the number density profiles along the LISN meridian using GPS TEC values and VIPIR bottomside densities and regularization algorithms [*Nygrén et al.*, 1997; *Lee et al.*, 2007]. The detection and characterization of TIDs discussed here will help to investigate the role of gravity waves on seeding ESF. We plan to operate the VIPIR ionosondes in a mode amenable for the calculation of plasma drifts using Doppler information and the continuity equation and the motion of F layers during sunset. Two VIPIR ionosondes will be located ∼11–12° on both sides of the magnetic equator; to study the role of E_s layers on the onset and dynamics of ESF. We also intend to extract tide and planetary wave information using (1) regional maps of TEC that can provide evidence of the presence of semidiurnal tides, (2) E field values from all pairs of magnetometers in South America, and (3) plasma drifts measured by the LISN VIPIR ionosondes. Completion of these projects will provide the necessary scientific know-how to develop assimilation techniques that will become important pieces of a new predictive numerical and data ingestion model of the low-latitude ionosphere over South America.

6. Summary

[38] TEC measurements from the GPS receivers in the LISN distributed observatory were used together with several other receivers that operate in South America to gather the regional distribution of TEC enhancements that occur near midnight at low latitudes. It was shown that the N-MTECE of 11–12 March 2011 was formed by a receding equatorial anomaly driven by a reverse fountain effect acting in response to downward vertical drift. It was also suggested that meridional winds produce an asymmetry in the intensity of the crests controlling the final location of the region of enhanced TEC.

[39] The CCM method has been applied to stations separated by hundreds of km, as data collected at Huancayo, Cuzco, Piura, Iquitos, Ancon and Leticia were used to calculate the characteristics of TIDs. A large coherence was found between the TECP traces from all the adjacent stations, allowing us to determine the morphological characteristics of the TIDs. This result opens the possibility of using measurements of the TEC perturbations by the GPS receivers already deployed in South America to monitor TID activity.

[40] This paper has also presented the day-to-day variability of the TEC depletions over the South American continent for the years of 2008 and 2009. Observations of depletions during these years of low solar activity showed that the seasonal and longitudinal variability is comparable to that obtained in *Burke et al.* [2004]. It can be concluded that the climatology of depletions agree with *Tsunoda*'s [2010a] STBA hypothesis.

[41] The science highlights reported here speak of the usefulness of the LISN observatory to probe the disturbed and undisturbed low-latitude ionosphere over South America. The regional TEC climatology and day-to-day variability for different levels of solar and magnetic conditions and energy inputs from the thermosphere will be assessed and reported in the near future. It is indicated that the installation of four

VIPIR ionosondes will lead to new and important discoveries in equatorial Aeronomy.

[42] **Acknowledgments.** The authors would like to thank the International GNSS Service (IGS), Geocentric Reference System for the Americas (SIRGAS), and Michael Bevis from Ohio State University–Central and Southern Andes GPS Project (OSU-CAP) for providing GPS data. Hector Mora from the Colombian Institute of Geology and Mining (INGEOMINAS) provided RINEX files from the stations at Cucuta, Rioacha, Corozal, and Bahia Solano in Colombia. Data exchange was made possible under the frame of the international collaboration between the LISN project of Boston College and project GEORED of INGEOMINAS. One of the authors, C. E. Valladares, was partially supported by Air Force Research Laboratory contract FA8718-09-C-0041 and NSF grant ATM-0521487. Work done at Boston College was supported by the Air Force Office of Scientific Research. The Low-Latitude Ionospheric Sensor Network (LISN) is a project led by Boston College in collaboration with the Geophysical Institute of Peru and other institutions that provide information in benefit of the scientific community. We thank all organizations and persons that are supporting and operating receivers in LISN. We thank Robert Sheehan for his helpful comments and suggestions on the paper.

References

Aarons, J. (1993), The longitudinal morphology of equatorial F layer irregularities relevant to their occurrence, *Space Sci. Rev.*, *63*, 209–243, doi:10.1007/BF00750769.

Abdu, M. A., E. A. Kherani, I. S. Batista, E. R. de Paula, D. C. Fritts, and J. H. A. Sobral (2009), Gravity wave initiation of equatorial spread F/plasma bubble irregularities based on observational data from the SpreadFEx campaign, *Ann. Geophys.*, *27*, 2607–2622, doi:10.5194/angeo-27-2607-2009.

Afraimovich, E. L., et al. (1998), GPS radio interferometry of travelling ionospheric disturbances, *J. Atmos. Sol. Terr. Phys.*, *60*, 1205–1223, doi:10.1016/S1364-6826(98)00074-1.

Afraimovich, E. L., et al. (2000), Determining parameters of large-scale traveling ionospheric disturbances of auroral origin using GPS-arrays, *J. Atmos. Sol. Terr. Phys.*, *62*, 553–565, doi:10.1016/S1364-6826(00)00011-0.

Afraimovich, E. L., N. P. Perevalova, and S. V. Voyeikov (2003), Traveling wave packets of total electron content disturbances as deduced from global GPS network data, *J. Atmos. Sol. Terr. Phys.*, *65*(11–13), 1245–1262, doi:10.1016/j.jastp.2003.08.007.

Balan, N., and G. J. Bailey (1995), Equatorial plasma fountain and its effects: Possibility of an additional layer, *J. Geophys. Res.*, *100*, 21,421–21,432, doi:10.1029/95JA01555.

Balan, N., and P. B. Rao (1984), Relationship between nighttime total electron content enhancements and VHF scintillations at the equator, *J. Geophys. Res.*, *89*, 9009–9013, doi:10.1029/JA089iA10p09009.

Burke, W. J., L. C. Gentile, C. Y. Huang, C. E. Valladares, and S. Y. Su (2004), Longitudinal variability of equatorial plasma bubbles observed by DMSP and ROCSAT-1, *J. Geophys. Res.*, *109*, A12301, doi:10.1029/2004JA010583.

Chau, J. L., B. G. Fejer, and L. P. Goncharenko (2009a), Quiet variability of equatorial E × B drifts during a sudden stratospheric warming event, *Geophys. Res. Lett.*, *36*, L05101, doi:10.1029/2008GL036785.

Chau, J. L., M. A. Milla, and E. Kudeki (2009b), Multi-Frequency Radar studies of the equatorial 150-km region, paper presented at Twelfth International Workshop on Technical and Scientific Aspects of MST Radar, Can. Assoc. of Phys., London, Ont., Canada.

Chau, J. L., N. A. Aponte, E. Cabassa, M. P. Sulzer, L. P. Goncharenko, and S. A. Gonzalez (2010), Quiet time ionospheric variability over Arecibo during sudden stratospheric warming events, *J. Geophys. Res.*, *115*, A00G06, doi:10.1029/2010JA015378.

Conker, R. S., M. B. El-Arini, R. Lejeune, P. Doherty, and C. Valladares (2004), Description of a real-time algorithm for detecting ionospheric depletions for SBAS and the statistics of depletions in South America during the peak of the current solar cycle, paper presented at Beacon Satellite Symposium, Beacon Satell. Group, Int. Union Radio Sci., Trieste, Italy.

Doherty, P., A. J. Coster, and W. Murtagh (2004), Eye on the ionosphere: Space weather effects of October-November 2003, *GPS Solutions*, *8*, 267–271, doi:10.1007/s10291-004-0109-3.

Farley, D. T., B. B. Balsey, R. F. Woodman, and J. P. McClure (1970), Equatorial spread F: Implications of VHF radar observations, *J. Geophys. Res.*, *75*(34), 7199–7216, doi:10.1029/JA075i034p07199.

Fejer, B. G., J. W. Jensen, and S.-Y. Su (2008), Quiet time equatorial F region vertical plasma drift model derived from ROCSAT-1 observations, *J. Geophys. Res.*, *113*, A05304, doi:10.1029/2007JA012801.

Fritts, D. C., et al. (2008), Gravity wave and tidal influences on equatorial spread F based on observations during the Spread F Experiment (SpreadFEx), *Ann. Geophys.*, *26*, 3235–3252, doi:10.5194/angeo-26-3235-2008.

Goncharenko, L. P., A. J. Coster, J. L. Chau, and C. E. Valladares (2010), Impact of sudden stratospheric warmings on equatorial ionization anomaly, *J. Geophys. Res.*, *115*, A00G07, doi:10.1029/2010JA015400.

Ho, C. M., A. J. Manucci, L. Sparks, X. Pi, U. L. Lindqwister, B. D. Wilson, B. A. Iijima, and M. J. Reyes (1998), Ionospheric total electron content perturbations monitored by the GPS global network during two Northern Hemisphere winter storms, *J. Geophys. Res.*, *103*, 26409–26420, doi:10.1029/98JA01237.

Huang, C.-S., and M. C. Kelley (1996), Nonlinear evolution of equatorial spread F: 1. On the role of plasma instabilities and spatial resonance associated with gravity wave seeding, *J. Geophys. Res.*, *101*(A1), 283–292, doi:10.1029/95JA02211.

Huang, C. Y., W. J. Burke, J. S. Machuzak, L. C. Gentile, and P. J. Sultan (2001), DMSP observations of equatorial plasma bubbles in the topside ionosphere near solar maximum, *J. Geophys. Res.*, *106*, 8131–8142, doi:10.1029/2000JA000319.

Hysell, D. L., and J. D. Burcham (1998), JULIA radar studies of equatorial spread F, *J. Geophys. Res.*, *103*, 29,155–29,167, doi:10.1029/98JA02655.

Kirkland, M. W., and A. R. Jacobson (1998), Drift-parallax determination of the altitude of traveling ionospheric disturbances observed with the Los Alamos radio-beacon interferometer, *Radio Sci.*, *33*(6), 1807–1825, doi:10.1029/98RS02033.

Kudeki, E., and S. Bhattacharyya (1999), Post-sunset vortex in equatorial *F* region plasma drifts and implications for bottomside spread-F, *J. Geophys. Res.*, *104*, 28,163–28,170, doi:10.1029/1998JA900111.

Kudeki, E., A. Akgiray, M. Milla, J. L. Chau, and D. L. Hysell, (2007), Equatorial spread-F initiation: Post-sunset vortex, thermospheric winds, gravity waves, *J. Atmos. Sol. Terr. Phys.*, *69*, 2416–2427.

Lee, J. K., F. Kamalabadi, and J. J. Makela (2007), Localized three-dimensional ionospheric tomography with GPS ground receiver measurements, *Radio Sci.*, *42*, RS4018, doi:10.1029/2006RS003543.

Nygrén, T., M. Markkanen, M. Lehtinen, E. Tereshchenko, and B. Khudukon (1997), Stochastic inversion in ionospheric radiotomography, *Radio Sci.*, *32*(6), 2359–2372, doi:10.1029/97RS02915.

Pacheco, E. E., R. A. Heelis, and S.-Y. Su (2010), Quiet time meridional (vertical) ion drifts at low and middle latitudes observed by ROCSAT-1, *J. Geophys. Res.*, *115*, A09308, doi:10.1029/2009JA015108.

Portillo, A., M. Herraiz, S. M. Radicella, and L. Ciraolo (2008), Equatorial plasma bubbles studied using African slant total electron content observations, *J. Atmos. Sol. Terr. Phys.*, *70*, 907–917, doi:10.1016/j.jastp.2007.05.019.

Rama Rao, P. V. S., S. Gopi Krishna, K. Niranjan, and D. S. V. V. D. Prasad (2006), Study of spatial and temporal characteristics of L-band scintillations over the Indian low-latitude region and their possible effects on GPS navigation, *Ann. Geophys.*, *24*, 1567–1580, doi:10.5194/angeo-24-1567-2006.

Reinisch, B. W., X. Huang, I. A. Galkin, V. Paznukhov, and A. Kozlov (2005), Recent advances in real-time analysis of ionograms and ionospheric drift measurements with digisondes, *J. Atmos. Sol. Terr. Phys.*, *67*(12), 1054–1062, doi:10.1016/j.jastp.2005.01.009.

Röttger, J. (1973), Wave-like structures of large-scale equatorial spread-F irregularities, *J. Atmos. Terr. Phys.*, *35*, 1195–1196, doi:10.1016/0021-9169(73)90016-0.

Saito, A., T. Iyemori, and M. Takeda (1998), Evolutionary process of 10 kilometer scale irregularities in the nighttime midlatitude ionosphere, *J. Geophys. Res.*, *103*(A3), 3993–4000, doi:10.1029/97JA02517.

Sardón, E., and N. Zarraoa (1997), Estimation of total electron content using GPS data: How stable are the differential satellite and receiver instrumental biases?, *Radio Sci.*, *32*(5), 1899–1910, doi:10.1029/97RS01457.

Seemala, G. K., and C. E. Valladares (2011), Statistics of total electron content depletions observed over the South American continent for the year 2008, *Radio Sci.*, *46*, RS5019, doi:10.1029/2011RS004722.

Shiokawa, K., Y. Otsuka, T. Ogawa, N. Balan, K. Igarashi, A. J. Ridley, D. J. Knipp, A. Saito, and K. Yumoto (2002), A large-scale traveling ionospheric disturbance during the magnetic storm of 15 September 1999, *J. Geophys. Res.*, *107*(A6), 1088, doi:10.1029/2001JA000245.

Sridharan, R., R. Sekar, and S. Gurubaran (1993), Two-dimensional high-resolution imaging of the equatorial plasma fountain, *J. Atmos. Terr. Phys.*, *55*, 1661–1663, doi:10.1016/0021-9169(93)90170-4.

Sultan, P. J. (1996), Linear theory and modeling of the Rayleigh-Taylor instability leading to occurrence of equatorial spread F, *J. Geophys. Res.*, *101*, 26,875–26,891, doi:10.1029/96JA00682.

Tsunoda, R. T. (1985), Control of the seasonal and longitudinal occurrence of equatorial scintillations by the longitudinal gradient in the integrated

E region Pedersen conductivity, *J. Geophys. Res.*, *90*, 447–456, doi:10.1029/JA090iA01p00447.

Tsunoda, R. T. (2005), On the enigma of day-to-day variability in equatorial spread F, *Geophys. Res. Lett.*, *32*, L08103, doi:10.1029/2005GL022512.

Tsunoda, R. T. (2006), Day-to-day variability in equatorial spread F: Is there some physics missing?, *Geophys. Res. Lett.*, *33*, L16106, doi:10.1029/2006GL025956.

Tsunoda, R. T. (2010a), On equatorial spread *F*: Establishing a seeding hypothesis, *J. Geophys. Res.*, *115*, A12303, doi:10.1029/2010JA015564.

Tsunoda, R. T. (2010b), On seeding equatorial spread *F*: Circular gravity waves, *Geophys. Res. Lett.*, *37*, L10104, doi:10.1029/2010GL043422.

Vadas, S. L. (2007), Horizontal and vertical propagation and dissipation of gravity waves in the thermosphere from lower atmospheric and thermospheric sources, *J. Geophys. Res.*, *112*, A06305, doi:10.1029/2006JA011845.

Valladares, C. E., and M. A. Hei (2012), Measurement of the characteristics of TIDs using small and regional networks of GPS receivers during the campaign of 17–30 July of 2008, *Int. J. Geophys.*, doi:10.1155/2012/548784, in press.

Valladares, C. E., W. B. Hanson, J. P. McClure, and B. L. Cragin (1983), Bottomside sinusoidal irregularities in the equatorial F region, *J. Geophys. Res.*, *88*, 8025–8042, doi:10.1029/JA088iA10p08025.

Valladares, C. E., J. Villalobos, M. P. Hagan, and R. Sheehan (2004), Latitudinal extension of low-latitude scintillations measured with a network of GPS receivers, *Ann. Geophys.*, *22*, 3155–3175, doi:10.5194/angeo-22-3155-2004.

Valladares, C. E., J. Villalobos, M. A. Hei, R. Sheehan Su. Basu, E. MacKenzie, P. H. Doherty, and V. H. Rios (2009), Simultaneous observation of traveling ionospheric disturbances in the northern and southern hemispheres, *Ann. Geophys.*, *27*, 1501–1508.

Woodman, R. F. (1970), Vertical drift velocities and east–west electric fields at the magnetic equator, *J. Geophys. Res.*, *75*, 6249–6259, doi:10.1029/JA075i031p06249.

Woodman, R. F., and C. LaHoz (1976), Radar observations of F region equatorial irregularities, *J. Geophys. Res.*, *81*, 5447–5466, doi:10.1029/JA081i031p05447.